Optimization And Finite Element Simulation of Friction Stir Butt Welding of AA4047 Aluminium Plates

Wazeda Begum[1], Rahul Prajapati[2] and Swagatika Acharya[3]

[1,3]Assistant Professor, Department of Mechanical Engineering, Gandhi Institute For Technology (GIFT), Bhubaneswar
[2]Assistant Professor, Department of Mechanical Engineering, Gandhi Engineering College, Bhubaneswar

Publishing Date: Dec 31, 2015

Abstract – The present paper focus on the finite element simulation of the friction stir welding (FSW) of AA4047 Aluminium plates based on the commercial numerical codes of Altair Hyperworks with an objective to investigate the complex interaction of thermo-mechanical process characteristics of FSW. A 3D finite element model (FEM) heat transfer model has been proposed and temperature and pressure distribution along with the variation of flow stress during the welding of plates was critically investigated. Also, Taguchi L9 orthogonal array technique was used to optimize the process parameters for obtaining defect-free high-quality welds. It is expected that the present work will be useful for understanding the underlying physics and thermo-mechanical mechanism of FSW.

Keywords- Friction stir welding, Finite element simulation, Tool pin diameter, Tool rotational speed, Tool feed rate, Tensile strength, Aluminium plate.

I. INTRODUCTION

Friction Stir Welding (FSW) is an advanced energy-efficient solid state joining process that involves joining of metals without fusion or filler materials [1]. The chief advantages of the process are its ability to weld difficult-to-weld materials like aluminium alloys, magnesium, copper etc and environmentally friendliness as it does not produce any harmful gases and spatter. These advantages results from the fact that process is carried much below the melting temperature of the materials to be joined [2]. The basic principle involved during the joining is the mechanical intermixing of metal at the place of joint and transforming them into a softened state that allows the metal to be fused with each other under mechanical pressure. The joined material is plasticized (without melting) due to heat generated by the friction between the surface of the plates to be welded and the contact surface of a specially designed tool, which is composed of two main parts; shoulder and pin. Shoulder is responsible for the generation of heat and for containing the plasticized material in the weld zone, while pin mixes the material of the components to be welded, thus creating a defect-free joint characterized by good mechanical properties [3] and [4]. The process involves complex interactions between large numbers of simultaneous thermo-mechanical parameters, which affect the heating and cooling rates, plastic deformation and flow, dynamic recrystallization phenomena and the mechanical integrity of the joint [5] and [6]. This demands an efficient design of the FSW tool geometry (tool pin diameter and length), as well as proper control of various FSW characteristics (tool feed rate, tool rotational speed) to achieve defect-free joint with superior mechanical properties. One way to achieve this is by the finite element modeling of FSW process [7] and [8].

Although much research and development work has been reported for FSW processes; not much work has been carried in the area of FEM simulation of FSW processes. The primary reason is the physics behind the process, which very complex in nature and includes mechanical heat generation along with heat and mass transfer mechanisms [9]. During FSW, conduction of heat is aided by the plastic flow of substrate close to the rotating tool. The heat and mass transfer depend on the material properties, as well as welding parameters including rotational and welding speeds of the tool and its geometry. These factors have great influence on the weld quality by controlling heat generation, heat transmission and stirring of the metal [10] and [11]. It can be stated that in FSW, the joining takes place by extrusion and forging of the metals at high strain rates [12]. Keeping these in mind, the authors gave an attempt to formulate numerical codes for FEM of FSW process with an aim to investigate the complex interaction of the thermo-mechanical characteristics. A 3D finite element heat transfer model using the commercial numerical codes of Altair Hyperworks has been proposed for the same and was validated with the experimental results. Also, Taguchi L9 orthogonal array technique was utilized to optimize the process parameters like tool rotational speed, tool feed rate and tool pin diameter to get a high-strength butt joints. It is expected that the present research work will be highly beneficial for the FSW process.

II. EXPERIMENTAL INVESTIGATIONS

The friction stir welding system consists of FSW tool, workpiece and fixture for holding workpiece. The detail of FSW components and typical composition of 4047 aluminium alloy workpiece considered under the present research work are illustrated in table 1 and 2 respectively. Figure 1 gives the illustration of FSW tool, Aluminium workpiece and fixture plate and FSW process.

TABLE 1. DIMENSIONS OF FSW COMPONENTS

Sl. No.	FSW Components		Dimensions
1.	FSW Tool (Mild Steel)	Tool Shoulder	Length: 70mm, Diameter: 24mm
		Tool Pin (Straight Cylindrical)	Length: 7 mm; Diameter: 6mm, 7mm & 8mm
2.	Workpiece (AA 4047 Silicon based Aluminium Alloy)	Rectangular Plate	Length: 50mm, Width: 120mm, Thickness: 10mm
3.	Fixture (Mild Steel)	Rectangular Plate	Thickness: 20mm with central groove of 2mm depth and 10mm width

TABLE 2. TYPICAL COMPOSITION OF AA 4047 ALUMINIUM ALLOY

Element	Si	Fe	Cu	Mn	Mg	Zn	Ti	Al
%	4.5	0.8	0.3	0.05	0.05	0.1	0.2	Remaining

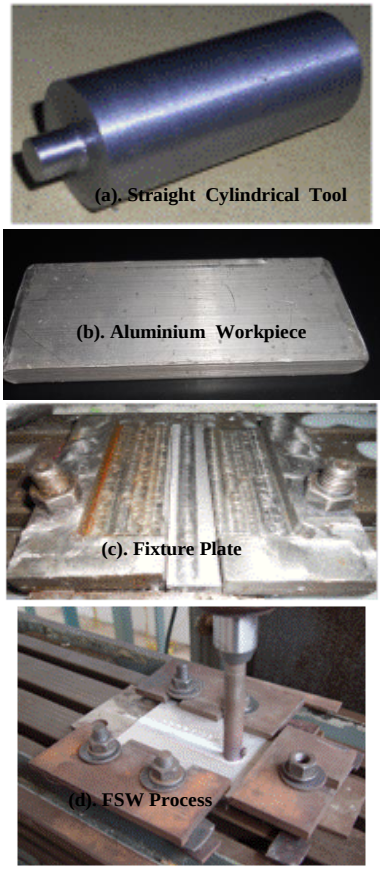

Figure 1. Illustration of FSW components.

Table 3 shows the various levels of FSW process parameters considered under the present research. It can be seen that three different levels of tool rotational speed, feed rate and tool pin diameter have been considered to study the effect of these factors on the weld quality. Figure 2 show the sample illustration of the butt welded Aluminium plates after FSW process. As seen from the figure 2(a), a tunnel like void is seen in the bottom of the weld line at the forwarding side. As seen from figure 2(b), these voids get minimized as higher levels of process parameters are selected for the experiment. Finally, the quality of welded joint is best seen in figure 2(c), where all process parameters are at highest level, i.e. tool rotational speed of 1100rpm, tool feed rate of 55mm/min and pin diameter of 8mm. This indicates that increase in the tool rotational speed, tool traverse rate and tool pin diameter minimizes the void formation in the stirring zone and FSW butt welded joints are of best quality.

TABLE 3. FSW PROCESS PARAMETERS LEVELS

Sl. No.	Welding Parameters	Level 1	Level 2	Level 3
1.	Tool Rotational Speed 'N' (rpm)	500	710	1100
2.	Tool Feed 'F' (mm/min)	45	50	55
3.	Pin Diameter 'D' (mm)	6	7	8

Figure 2. FSW Butt Welded Aluminium Plates.

The solid-state nature of the FSW process, combined with its unusual tool results in a highly characteristic microstructure, which can be classified as unaffected material zone, heat-affected zone, thermo-mechanically affected zone and weld nugget [13] and [14]. The weld quality is primarily affected by weld nugget zone, which is basically a dynamically re-crystallized region of heavily deformed material. The grains within this zone are roughly equiaxed and often an order of magnitude smaller than the grains in the parent material [15] and [16]. A unique feature of this zone is the common occurrence of several concentric rings referred as

"onion rings", which originate due to stirring action of the FSW tool pin [17], [18] and [19]. Figure 3 shows the photomicrograph of the SEM image of the stir zone on the Aluminium workpiece showing the portion of "onion rings" at 1000x.

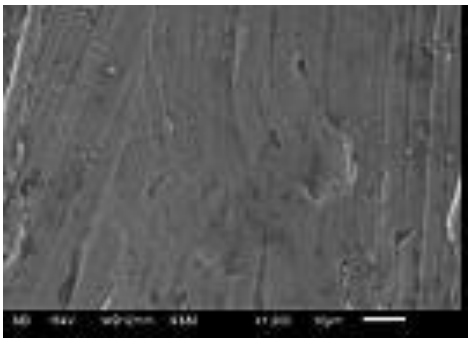

Figure 3. SEM Image of Stir Zone.

III. OPTIMIZATION OF FSW

To evaluate the optimum conditions of FSW process parameters with respect to FSW butt weld quality; tensile testing of the specimens were carried and the same were optimized using Taguchi L9 orthogonal array technique, which considered three control parameters each at three levels (refer table 3) [20] and [21]. The experimental runs with associated tensile strength results and S/N ratio are reported in table 4. The objective of using Taguchi technique was to reduce the time and cost to evaluate the optimum welding conditions [22]. Results of the FSW experimental runs were studied by using the S/N and ANOVA technique was used to analyze and optimize the process parameters for tensile strength data obtained. The hypothesis considered for the present optimization was "higher-the-better" performance characteristic for tensile strength. The S/N ratio for higher-the-better characteristics was calculated using following equation [23]:

$$S/N_{LB} = -10log_{10}[\frac{1}{n}\sum_{i=1}^{n}(\frac{1}{Y_i^2})] \quad (1)$$

where, 'Y' is tensile strength of specimen for i^{th} test in the trial.

TABLE 4. EXPERIMENTAL RESULTS FOR TENSILE STRENGTH AND S/N RATIO OF FSW BUTT WELDS

Runs	N	F	D	Tensile Strength	S/N ratio
1	500	45	6	103	40.2567
2	500	50	7	107	40.5877
3	500	55	8	98	39.8245
4	710	45	8	115	41.214
5	710	50	6	119	41.5109
6	710	55	7	117	41.3637
7	1100	45	7	122	41.7272
8	1100	50	8	121	41.6557
9	1100	55	6	127	42.0761

It is possible to separate out the effect of each process parameter at different levels as the experimental design is orthogonal, e.g. mean S/N ratio for the tool rotational speed at levels 1, 2 and 3 can be calculated by averaging the S/N ratios for the experiments 1-3, 4-6, and 7-9 respectively. Similarly, the mean S/N ratio for each level of the other process parameters can be computed. The mean S/N ratio for each level of the process parameters summarized for tensile strength is shown in table 5 and the corresponding graph is shown in figure 4. The larger S/N ratio yields the optimal parametric combination for tensile strength, i.e. tool rotational speed at level 3, tool feed rate at level 3 and tool pin diameter at level 3 (N3-F3-D3).

TABLE 5. MEAN S/N RATIO FOR TENSILE STRENGTH

Level	N	F	D
1	40.22	41.07	41.09
2	41.36	41.25	41.29
3	41.82	41.09	41.02
Max-min	1.6	0.19	0.27
Rank	1	3	2

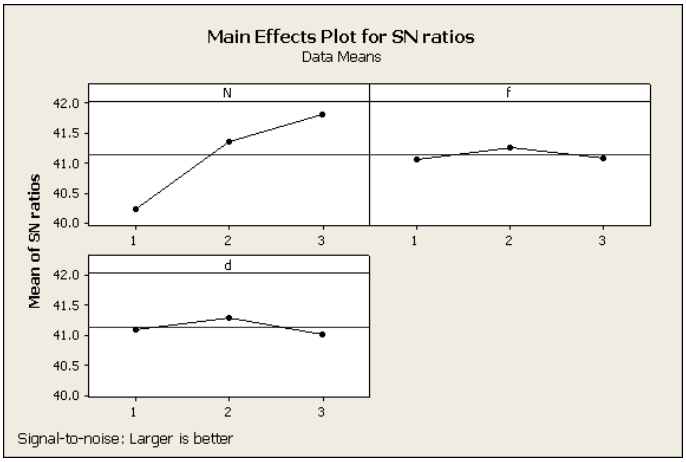

Figure 4. Mean S/N graph for tensile strength.

Table 6 shows the results of ANOVA test for tensile strength of FSW butt welded joints to find the statistical significance of process parameter on response. Confirmation experiment has been carried out to predict and verify the improvement of the performance characteristics using the optimal combination of process parameter. Table 7 shows the results of the confirmation experiment using the optimal process parameters and initial process parameters. The increase of S/N ratio from the initial process parameters to the optimal process parameters is 16.478%. The improvement of the S/N ratio for the individual performance characteristics is shown in table 8. Thus, based on the results of confirmation test, the

tensile strength of the FSW butt welded joint is increased 6.66 times.

TABLE 6. ANALYSIS OF VARIANCE FOR TENSILE STRENGTH FROM S/N RATIO

Source	DF	SS	MS	F	P
N	2	64.72	32.36	1.12	0.471
F	2	202.1	101.05	3.50	0.022
D	2	90.95	45.48	1.58	0.388
Error	2	57.73	28.87		
Total	8	415.5			

TABLE 7. RESULTS OF CONFIRMATION EXPERIMENT FOR TENSILE STRENGTH

	Initial Process Parameters	Optimal Process Parameters	
		Prediction	Experiment
Level	P1-N1-G1	P3-N3-G3	P3-N3-G3
Tensile Strength	0.048		0.32
S/N Ratio	-26.375	-7.06	-9.897
Improvement of S/N Ratio	16.478		

TABLE 8. IMPROVEMENT OF S/N RATIO FOR INDIVIDUAL PERFORMANCE CHARACTERISTICS

ANOVA						
Source	**DF**	**Seq SS**	**Adj SS**	**Adj MS**	**F**	**P**
N	2	672.67	672.67	336.33	16.02	0.039
F	2	8.67	8.67	4.33	0.21	0.829
D	2	18.67	18.67	9.33	0.44	0.692
Error	2	42	42	21		
Total	8	742				
		R-Sq	0.9434			

IV. FINITE ELEMENT MODELING

The objective FEM analysis of FSW was to develop a computational thermal model for friction stir butt weld based on the experimental data using commercial numerical codes of Altair Hyperworks [24]. The geometric model was developed using a preprocessor Altair Hyperextrude and the corresponding geometrical output file was solved using Hyperextrude solver. The temperature and pressure distribution on the workpiece plates during FSW process in form of temperature and pressure contour plots were generated using the geometric solver. The material property of the workpiece plate was selected from the material library as Aluminium 4000 series of AA4047 type of alloy and the material properties used in the present simulation is shown in table 9. The solid models of Aluminium plates along with FSW tool, shoulder and pin with 3D solid hexagonal finite elements having required dimensions is shown in figure 5. The aluminium plates, tool shoulder and tool pin were meshed with the same mesh parameters with 25 numbers of 3D solid hexagonal elements. Thus, in total 200 elements with 1209 nodes was generated in the present analysis. The FSW tool was modeled as tool steel of H13 series. The boundary conditions of FSW butt weld thermal model was specified through FSW Altair Hyperextrude codes, which were dependent on the overall heat transfer coefficient. Convective heat losses occurred across all the free surfaces of the workpiece and conduction losses occurred from the workpiece surface to the backup plates. Also, a small heat loss occurred to the tool and minimal heat loss through radiation from the workpiece surface. As the difference in the process temperatures and ambient temperatures were relatively low, the percentage of heat loss due to radiation was low and hence, the effective radiative heat losses were neglected [25].

TABLE 9. MATERIAL PROPERTIES OF THE BUTT JOINT

Sl. No.	Property	Value
1.	Workpiece Material	AA4047 Aluminium
2.	Tool Material	Tool Steel (H13 series)
3.	Workpiece Density	0.096 lb/in^3
4.	Thermal x-Conductivity (x, y & z axes)	243 W m^{-1} K^{-1}

Figure 6 shows the variation of temperature along the FSW butt welded joint line. It can be observed from the figure that the highest temperature of about 680^{0}C was attained at the center of the stirring zone, whereas HAZ experienced temperature of about 400^{0}C. It can be clearly seen that HAZ is elliptical in shape with its major axis along the line of the welded joint with center of stirring as the one of the ellipse centers. Also, the elliptical temperature gradient increases with the distance from the stirring zone and reduction of temperature. The workpiece on the preceding side of the tool travel is least affected, where as the forwarding side of the workpiece is highly affected by the heat generated during FSW process.

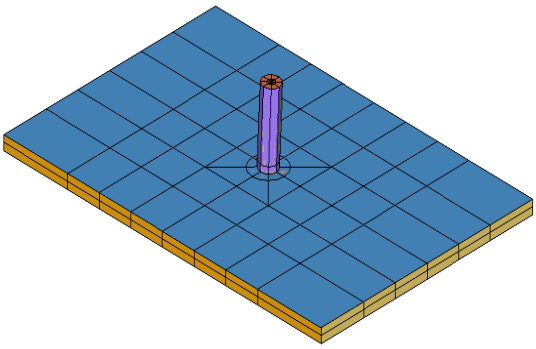

Figure 5. Finite element model of FSW tool and plate.

Figure 7 shows the distribution of the pressure on the workpiece surface during FSW process. The presence of the pressure indicates and confirms that FSW is basically a themo-mechanical welding process, where mechanical pressure plays a significant role during welding of the plates. It can be clearly observed that welding pressure of about 420MPa is generated at the center of the stirring zone, whereas the nearby HAZ area are under influence of pressure in the order of 200 - 300MPa. The shape of the pressure affected zone is approximately triangular in shape with one of the vertices being at the center of the stirring zone. Also, the pressure gradient are symmetrical to the weld line and predominantly present in the forward direction of the welding tool, whereas the preceding areas on the workpiece are least affected.

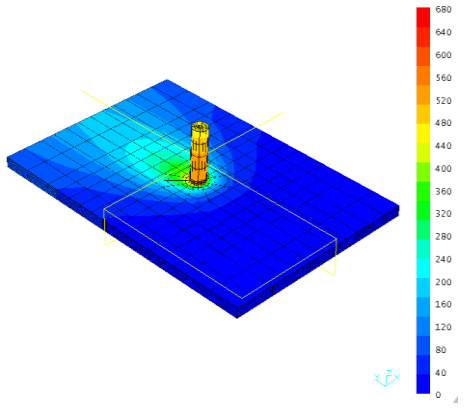

Figure 6. Variation of temperature (^{o}C) along tool travel direction.

The flow stress variation during the FSW process is shown in the figure 8. It shows that the flow stress value is maximum at the forwarding direction of the welding tool along the direction of tool traverse and is found to be about 260MPa at the center of the stirring zone. It was interesting to note that flow stress being material property and dependent on the working temperature is found to be lower that the welding pressure imposed at the same regions. This confirms the significance of welding pressure during FSW processes and the need to investigate its effects on the FSW process parameters.

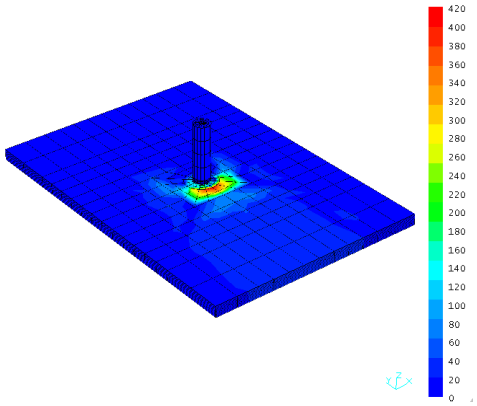

Figure 7. Variation of pressure (MPa) along tool travel direction.

V. CONCLUSIONS

From the preceding investigations, following important conclusions can be drawn:

- Experimental investigation for study of the effect of various FSW process parameters on tensile strength of the welded joint was successfully performed. Results showed that tool rotational speed of 1100rpm, tool feed rate of 55mm/min and pin diameter of 8mm have been found to be optimum with respect to the weld quality.
- Taguchi L9 orthogonal array optimization was performed to find out the optimal combination of the FSW process parameters and it was found that tool rotational speed of 1100rpm, tool traverse speed of 55mm/min and tool pin diameter of 8mm resulted in the maximum tensile strength of 41.82MPa. The improvement in S/N ratio from the initial process parameters to the optimal process parameters was found to be 16.478%. Also, the confirmation tests were performed by using ANNOVA tests and tensile strength was found to increase by 6.66 times the original value.
- FEM simulation of FSW process using Hyperworks software for investigation of the complex interaction of process parameters and thermo-mechanical characteristics during butt welding of Aluminium plates was successfully performed. A 3D FEM heat transfer model was also proposed and temperature and pressure distribution along with the variation of flow stress during the welding of plates was critically investigated. It was found that both welding temperature and pressure were maximum at the center of the stirring zone. The temperature gradient was found to be elliptical in nature with one of its center as the center of the stirring zone, where as the pressure gradient was found to vary in triangular in nature with one of its vertex as the center of the stirring zone. Also, both the distributions / gradients were found to be symmetrical about the weld line and have predominant effect in the forward region of the welding tool travel and the preceding regions were least affected.

AA4047 Aluminium alloy have distinct advantage of environment friendliness, high strength to weight ratio and high resistance to corrosion; but difficulty in welding makes it unsuitable for most applications. Since it can be welded easily and economically by FSW process, it is finding some applications like speed regulator in 3-phase motor, rifle scope mount, camera mounts etc. finally, it is expected that the present work will enhance the understanding of the FSW process and will definitely open-up the investigations in this area using various simulation tools, as not much work has been reported on the investigations of FSW using these tools.

REFERENCES

[1] W. Dequing, and L. Shuhua, "Study of Friction stir welding of aluminum," J. of Mater. Sci., vol. 39, pp. 1689-1693, 2004.

[2] Z.Y. Ma, "Friction stir processing technology: a review," Metall. and Mater.Trans., vol.39, pp. 642-658, 2008.

[3] H.K.D.H. Bhadesia, and T. DebRoy, "Critical assessment: friction stir welding of steels," Sc. and Tech. of Welding and Joining, vol. 14, pp. 193-194, 2009.

[4] T.J. Lienert, W.L. Stellwag, B.B. Grimmett, and R.W. Warke, "Friction Stir welding studies on mild steel," The Welding J., The American Welding Society and Welding Research Council, pp. 1S-9S, 2003.

[5] J. Adamowski, and M. Szkodo, "Friction-stir-welds (FSW) of aluminum alloy AW6082-T6," J. of Achievements in Mat. and Manuf. Engg., vol. 20, pp. 403-406, 2007.

[6] T. Sakthivel, G.S. Senegar, and J. Mukhopadhyay, "Effect of welding speed on micro-structure and mechanical properties of friction-stir welded aluminum," Int. J. of Adv. Manuf. Tech., vol. 43, pp. 468-473, 2008.

[7] M. Boz, and A. Kurt, "The Influence of stirrer geometry on bonding and mechanical properties in friction stir welding process," J. of Mater. and Des., vol. 25, pp. 343-347, 2004.

[8] S.L.A.C.De Filippis, and P. Cavaliere, "Influence of shoulder geometry on microstructure and mechanical properties of friction stir welded 6082 aluminum alloy," J. for Mater. and Des., vol. 28, pp. 1124-1129, 2007.

[9] M.B. Durdanovic, M.M. Mijajloric, D.S. Milcic, and D.S. Stamenkovic, "Heat generation during friction-stir-welding (FSW) process," Tribology in Ind., vol. 31, pp. 8-14, 2009.

[10] Y.M. Hwang, Z.W. Kang, Y.C. Chiou, and H.H. Hsu, "Experimental study on temperature distributions within the workpiece during friction stir welding of aluminum alloys," Int. J. of Mach. Tools & Manuf., vol. 48, pp. 778-787, 2008.

[11] H. Fujii, C. Ling, M. Maeda, and K. Nogi, "Effect of tool shape on mechanical properties and microstructure of friction stir welded aluminum alloys,", J. of Mater. Sci. and Engg., vol. 419, pp. 25-31, 2006.

[12] E. Cerri, and P. Leo, "Warm and room temperature deformation of friction stir welded thin aluminum sheets," J. for Mater. and Des., vol. 31, pp. 1392-1402, 2009.

[13] R.W. Fonda, J.A. Wert, A.P. Reynolds, and W. Tang, "Initial microstructural evolution during friction stir welding," Mater. Sc. and Tech., vol. 19, pp. 175-177, 2007

[14] T.R. McNelley, S. Swaminathan, and J.Q. Su, "Recrystallization mechanisms during friction stir welding/processing of aluminum alloys," Elsevier Science Ltd., vol. 58, 2008, 349-354, 2008.

[15] Y.G. Kim, H. Fujii, T. Tsumura, T. Komazaki, and K. Nakata, "Effect of welding parameters on microstructure in the stir zone of FSW joints of aluminum die casting alloy," J. for Mater. Letters, vol. 60, pp. 3830-3837, 2006.

[16] C.G. Rhodes, M.W. Mahoney, W.H. Bingel, and M. Calabrese, "Fine-grain evolution in friction-stir processed 7050 aluminum," Scripta Materialia, vol. 48, pp. 1451-1455, 2003.

[17] Y.S. Sato, H.K. Ikeda, M. Enomoto, S. Jogan, and T. Hashimoto, "Microtexture in the friction stir weld of aluminum alloy," Metall. and Mater. Trans., vol. 32, pp. 941-948, 2001.

[18] R.W. Fonda, and J.F. Bingert, "Micro-structural evolution in the heat-affected zone of a friction stir weld," Metall. and Mater. Trans., vol. 35, pp. 1487-1499, 2004

[19] E. Sukedai, T. Maebara, and T. Yokayama, "Micro-structure analysis of a friction-stir welded 2024 aluminium alloy using electron microscopy," Mater. Sc., vol. 2, pp. 673-674, 2008.

[20] F. Sarsilmaz, and U. Caydas, "Statistical analysis on mechanical properties of friction stir welded AA1050/AA5083 couples," Int. J. of Adv. Manuf. Tech., vol. 43, pp. 248-255, 2008.

[21] Y.S. Sato, and H. Kokawa, "Distribution of tensile property and micro-structure in friction stir weld of 6063 aluminum," Metall. and Mater. Trans., vol. 32, pp. 941-948, 2001.

[22] D.M. Rodrigues, A. Loureiro, C. Leitao, R.M. Leal, B.M. Chaparro, and P. Vilaca, "Influence of friction stir welding parameters on the micro-structural and mechanical properties of AA 6016-T4 thin welds," J. for Mater. and Des., vol. 30, pp. 1913-1921, 2009.

[23] M.M. Attallah, C.L. Davis, and M. Strangwood, "Microstructure-microhardness relationships in friction stir welded AA5251," J. of Mater. Sc., vol 42, pp. 7299-7306, 2007.

[24] Z. Meng, H. Chen, and X. Yue, "Study on optimization of stir head for FSW based on genetic algorithm," Int. Federation for Inf. Process., vol. 207, pp. 483-491, 2006.

[25] M. Cabibbo, H.J. McQueen, E. Evangelista, S. Spigarelli, M. Paola Di, and A. Falchero, "Microstructure and mechanical property studies of AA6056 friction stir welded plate," J. of Mater. Sci. and Engg., vol. 460-461, pp. 86-94, 2007.